Acousto–defect interaction in irradiated and non–irradiated silicon n^+–p–structure

O. Ya. Olikh,[1, a)] A. M. Gorb,[1] R. G. Chupryna,[1] and O. V. Pristay–Fenenkov[1]
Faculty of Physics, Taras Shevchenko National University of Kyiv, Kyiv 01601, Ukraine

(Dated: 22 November 2017)

The influence of ultrasound on I–V characteristics of non-irradiated silicon n^+–p–structures as well as silicon structures exposed to reactor neutrons or ^{60}Co gamma radiation have been investigated experimentally. It has been found that the ultrasound loading of n^+–p–structure leads to reversible change of shunt resistance, carrier lifetime, and ideality factor. Especially considerable acoustically induced alteration of ideality factor and the space charge region lifetime was observed in the irradiated samples. The experimental results were described by using the models of coupled defect level recombination, Shockley–Read–Hall recombination, and dislocation–induced impedance. The experimentally observed phenomena are associated with the increase of distance between coupled defects as well as the extension of carrier capture coefficient of complex point defects and dislocations. It has been shown that divacancies and vacancy–interstitial oxygen pairs are effectively modified by ultrasound in contrast to interstitial carbon–interstitial oxygen complexes.

Keywords: acousto–defect interaction, silicon, irradiation

I. INTRODUCTION

It is well known that ultrasound (US) can effectively interact with defects. As a defect engineering tool, US has the following advantages: (i) locality of action due to predominant absorption in the regions of lattice periodicity deviation; (ii) selectivity of influence, which depends on acoustic wave (AW) polarization and AW type; (iii) possibility to transform the defect system by applying resonance frequency; (iv) reversibility of the effect of low intensity AW.

In piezoelectric semiconductors, the acousto–defect interaction (ADI) is mainly determined by electric field that accompanies the vibration wave propagation. However, the ADI is also observed in such non–piezoelectric crystals as silicon, the basic material in microelectronics. It was experimentally observed that US can cause atomic diffusion,[1,2] transformation of native and impurity defects,[3–7] modification of interior surface states[8–10] and appearance of new defects[11,12] in Si structures. Defects are known to determine most of semiconductor devices characteristics. In particular, the ADI governs the variation of tunneling,[13,14] generation–recombination[15–17] and thermionic emission[18,19] currents in silicon barrier structures.

The change of population of impurity oscillator levels,[20] the displacement of impurity atoms with respect to their surroundings,[4,21,22] the decrease in the diffusion activation energy,[23] the local temperature increase caused by point defect clusters[24] as well as the US absorption by dislocations[16,25,26] are believed to be the main mechanisms of elastic vibration–defect interaction in non–piezoelectric crystals. However, to the best of our knowledge, there is no a comprehensive ADI theory for silicon suggested so far, the lack of experimental researches focused on acoustically induced (AI) effects being one of the main reasons.

The defects in silicon structures are not all acoustically active and can remain unmodified under the action of ultrasound. The ADI efficiency depends on defect type and structure.[8] For example, the force acting on the point defect in the crystal under US loading (USL) is determined by the relaxation of defect volume[21,22]. The alterations of semiconductor defects are most widely produced by using the well–studied irradiation method. On the one hand, the high–power US treatment of irradiated silicon structures has been shown[27–30] to result in residual changes in structure properties. This effect deals with AI annealing of radiation defects (RDs). On the other hand, irradiation can be the reason of reversible AI phenomenon initiation,[31,32] which is caused by formation of acoustically active RDs. Unfortunately, there are but a few reports on acoustically driven phenomenon in irradiated silicon structures.

The aim of our work is to investigate experimentally the AI electrical characteristic variation that takes place in non–irradiated and irradiated n^+–p–Si structures. For this purpose, the samples were irradiated by reactor neutrons and a ^{60}Co–gamma source rays. It is supposed that γ–rays introduce predominantly VO_i complex,[33–35] whereas neutrons mainly create vacancy clusters,[36,37] disordered regions,[38] and C_iO_i complexes.[35,39] Our work presents distinctions between AI effects in silicon structures with different RDs. The intensity of US applied was insufficient for a new defect formation, RD annealing or long distance (a many interatomic distance) diffusion. As a result, the complete recovery of characteristics was observed after AW propagation had stopped. To describe the processes in space charge region (SCR) and in the diode base as well as to study shunt

a)Electronic mail: olikh@univ.kiev.ua

TABLE I. The sample irradiation parameters.

Sample	Irradiation type	D (rad)	Ψ (cm^{-2})	NIEL[a] (MeV cm^2/g)	$\Psi \times$NIEL (MeV/g)
iSC	non	0	0	—	0
nSC	neutron	$4.5{\cdot}10^3$	$4{\cdot}10^{11}$	$2.04{\cdot}10^{-3}$	$8.2{\cdot}10^8$
g6SC	γ–^{60}Co	$1{\cdot}10^6$	$1.6{\cdot}10^{15}$	$1.07{\cdot}10^{-7}$	$1.7{\cdot}10^8$
g7SC	γ–^{60}Co	$1{\cdot}10^7$	$1.6{\cdot}10^{16}$	$1.07{\cdot}10^{-7}$	$1.7{\cdot}10^9$

[a] Ref. 44.

resistance, we used the models of coupled defect level recombination,[40,41] Shockley–Read–Hall (SRH) recombination and dislocation–induced impedance,[42,43] respectively. The observed AI phenomena are accounted for in terms of defect interaction with AW strain field.[21,22] Our research not only provides a better understanding of ADI but could also facilitates the development of acoustically controlled devices or radiation sensors.

II. EXPERIMENTAL AND CALCULATION DETAILS

n^+-p–Si structure was fabricated from 2 inch (300 μm thick) p–type boron doped Czochralski silicon wafer with <111> orientation and resistivity of 10 $\Omega{\cdot}$cm. The n^+ emitter with carrier concentration of about 10^{19} cm^{-3} and thickness of 0.5 μm was formed by phosphorus implantation. The front and rear aluminium electrodes were deposited by screen printing before rapid annealing. The samples used in the experiment were cut from the central part of the wafer and had the area of 2 cm^2. The samples were irradiated by reactor neutrons or by ^{60}Co γ–rays. The doses D, fluences Ψ, and sample labels are listed in Table I. To determine D and Ψ correlation, the data from Refs. 44 and 45 were used. The non–ionizing energy losses (NIEL) for neutron and γ–^{60}Co are also shown in Table I. Since the displacement damage effect is characterized by ($\Psi \cdot$ NIEL), a similar damage was expected in the investigated samples as well. To avoid the impact of long–term annealing, which is typical for neutron damaged structure,[35,36] the irradiated samples were stored for five years at room temperature before the measurements.

The dark forward current–voltage (I–V) characteristics of the samples both with and without USL were measured over a temperature range of 290–340 K. The temperature was controlled by differential copper–constantan thermocouple. Some of the obtained curves are shown in Fig. 1.

The double–diode model of n^+–p structure I–V characteristics is expressed in the following form:

$$I(V,T) = I_{SCR} + I_{base} + I_{sh}\,, \tag{1}$$

$$I_{SCR} = \frac{qAn_i d}{2\tau_g}\left\{\exp\left[\frac{q(V-IR_s)}{n_{\rm id}kT}\right]-1\right\}, \tag{2}$$

$$I_{base} = \frac{qAn_i^2}{p_p}\sqrt{\frac{\mu_n kT}{\tau_n}}\left\{\exp\left[\frac{q(V-IR_s)}{kT}\right]-1\right\}, \tag{3}$$

$$I_{sh} = (V-IR_s)/R_{sh}\,, \tag{4}$$

where I_{SCR} describes the overall SCR recombination, I_{base} is closely related to the recombination in quasi–neutral region, I_{sh} is the shunt current, A is the sample area, n_i is the intrinsic carrier concentration, τ_g is the SCR carrier lifetime, d is the SCR thickness:

$$d = \sqrt{\frac{2\varepsilon\varepsilon_0}{qp_p}\left[\frac{E_g}{q}-\frac{kT}{q}\ln\left(\frac{N_vN_c}{p_pn_n}\right)-\frac{2kT}{q}-V\right]}, \tag{5}$$

ε is the permittivity (11.7 for Si), p_p and n_n are the majority carrier concentration in p– and n–type regions, E_g is the semiconductor band gap, N_c and N_v are the effective densities of states in the conduction and valence bands; $n_{\rm id}$ is the ideality factor, R_s and R_{sh} are the series and shunt resistances, μ_n and τ_n are the mobility and lifetime of electron (minority carrier) in the diode base.

We used Eqs. (1)–(5) to fit the experimental data taking τ_g, τ_n, $n_{\rm id}$, R_{sh}, and R_s as the fitting parameters. Also, we used the known[46–48] temperature dependences of n_i, E_g, and μ_n. In the result, we obtained extremely good fit to the experimental data — see Fig. 1. In particular, for all the samples the value of R_s was found to be about 1 Ω. The broken lines in Fig. 1(a) show an example of the calculated contributions of I_{SCR}, I_{base}, and I_{sh} to the total current.

In case of USL, the transverse AWs with the frequency of 4.2 MHz, which were exited by using piezoelectric transducer, were applied to the samples at the base side in [111]–direction. The US intensities $W_{\rm US}$, amplitudes of lattice deformation $\xi_{\rm US}$ and lattice atom displacements $u_{\rm US}$ are listed in Table II. It was reported previously[6,7,19] that the characteristic time of change in silicon structure parameters under the US action did not exceed $2\cdot10^3$ s. In order to wait until the AI transitional period is competed the following experimental procedure was used. When USL started, the sample was first exposed to room temperature for 60 min and then the I–V measurement and the sample heating were started. In order to avoid the effect of piezoelectric field on I–V characteristics, the piezoelectric transducer was shielded.

Fig. 2 illustrates the reversibility of AI effects. The time interval between USL initiation and "during" measurement was longer than 60 min, the time interval between USL termination and "after" measurement was about 24 h. The data for nSC and g6SC are similar to those presented for iSC and g7SC.

The non-linear fittings were performed by using the differential evolution method.[49]

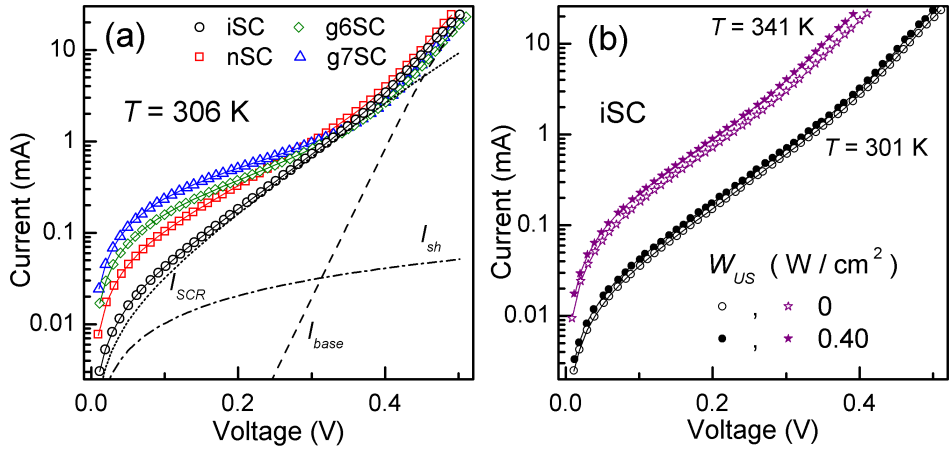

FIG. 1. Dark I–V characteristics measured (a) at 306 K for non–irradiated (circles), neutron–irradiated (squares) and gamma–irradiated (diamonds and triangles) structures without USL; (b) at 301 K (circles) and 341 K (asterisks) with (filled marks, Ui–2) and without (open marks) USL for the iSC. The marks are the experimental results, the solid lines are the curves fitted by Eqs. (1)–(5). The dashed, dotted and dot–dashed lines in (a) represent the calculated base, SCR and shunt components of total iSC current (black solid line).

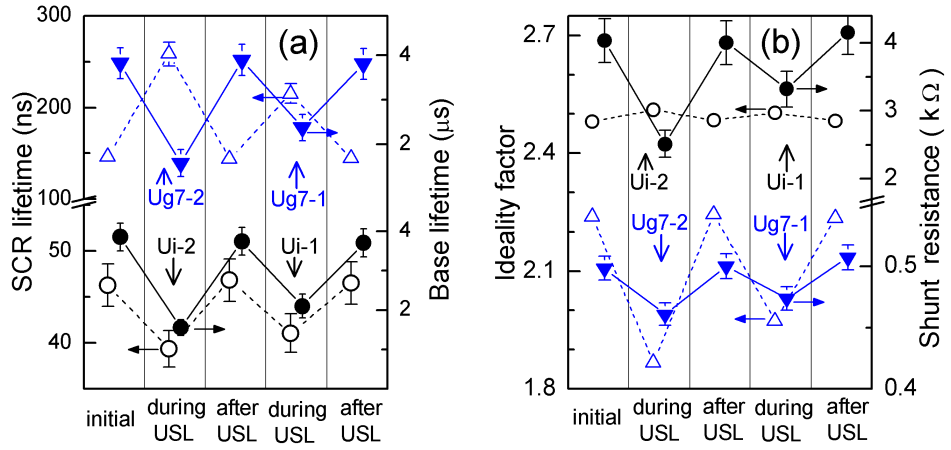

FIG. 2. SCR lifetime (a, left axis, open marks), base lifetime (a, right axis, filled marks), ideality factor (b, left axis, open marks) and shunt resistance (b, right axis, filled marks), obtained before, during and after USL at 330 K. Data for iSC (circles) and g7SC (triangles) are presented.

TABLE II. The ultrasound loading parameters.

Sample	W_{US} (W/cm^2)	ξ_{US} (10^{-6})	u_{US} (nm)	USL label
iSC	0.22	3.1	0.67	Ui–1
	0.40	4.2	0.91	Ui–2
nSC	0.24	3.2	0.70	Un–1
	0.40	4.2	0.91	Un–2
g6SC	0.38	4.1	0.89	Ug6–2
g7SC	0.19	2.9	0.63	Ug7–1
	0.37	4.0	0.87	Ug7–2

III. RESULTS AND DISCUSSION

A. Space charge region

The parameters of I–V characteristics associated with SCR phenomena are $n_{\rm id}$ and τ_g. The temperature dependences of ideality factor and SCR carrier lifetime are shown in Fig. 3 and Fig. 4,respectively.

As shown in Fig. 3, the ideality factor decreases with temperature increase, and the dependence of $n_{\rm id}$ on $1/T$ is close to linear. Thus, dependence $n_{\rm id}(T)$ can be expressed as

$$n_{\rm id}(T) = n_{\rm id,\infty} + T_{\rm id}/T\,. \qquad (6)$$

The thermoactivated growth of SCR lifetime is observed over the explored temperature range — see Fig. 4. The

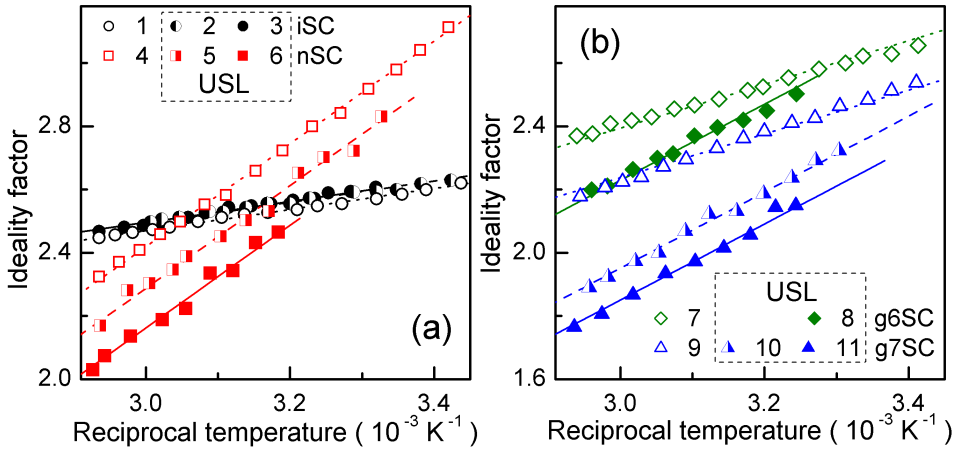

FIG. 3. Temperature dependences of ideality factor for non–irradiated (curves 1–3, circles), neutron–irradiated (4–6, squares) and γ–irradiated (7–11, diamonds and triangles) samples. The curves 1, 4, 7 and 9 (open marks) are obtained without USL, curves 2, 3, 5, 6, 8, 10, and 11 correspond to Ui–1, Ui–2, Un–1, Un–2, Ug6–2, Ug7–1, and Ug7–2 respectively. The marks are the experimental results, the lines are the fitted curves using Eq. (6).

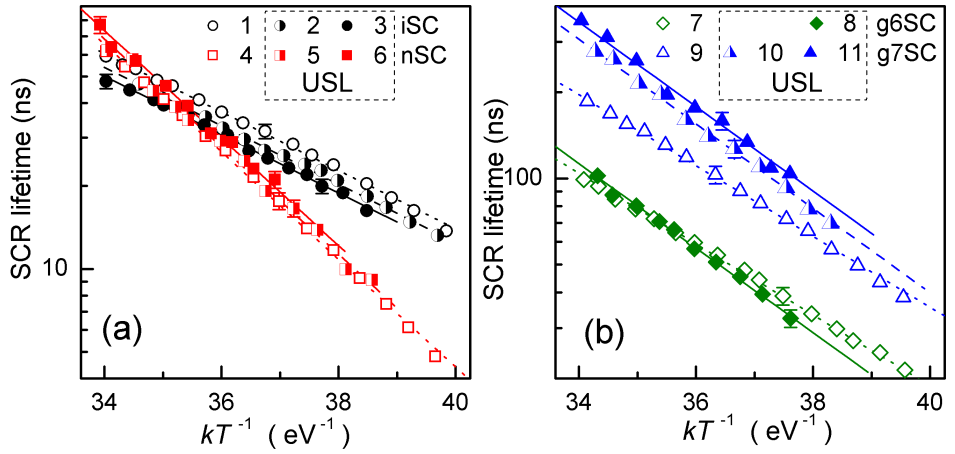

FIG. 4. Temperature dependences of SCR lifetime for non–irradiated (curves 1–3, circles), neutron–irradiated (4–6, squares) and γ–irradiated (7–11, diamonds and triangles) samples. The curves 1, 4, 7 and 9 (open marks) are obtained without USL, curves 2, 3, 5, 6, 8, 10, and 11 correspond to Ui–1, Ui–2, Un–1, Un–2, Ug6–2, Ug7–1, and Ug7–2 respectively. The marks are the experimental results, the lines are the fitted curves using Eq. (7).

temperature dependence of τ_g is well described by the following equation

$$\tau_g(T) = \tau_{g0} \exp\left(-\frac{E_{\tau g}}{kT}\right) . \qquad (7)$$

The values of $T_{\rm id}$ and $E_{\tau g}$ found for both non–irradiated and irradiated samples under USL as well as without USL are listed in Table III.

We would like to stress that
(i) irradiation leads to changes in $T_{\rm id}$ and $E_{\tau g}$, g6SC's characteristic temperature of ideality factor and SCR lifetime characteristic energy are closely related to those of g7SC under similar conditions;
(ii) USL affects $n_{\rm id}$ and τ_g values; the absolute AI changes of ideality factor $\Delta n_{\rm id} = n_{\rm id,US} - n_{{\rm id},in}$ and the relative AI changes of SCR lifetime $\varepsilon_{\tau g} = (\tau_{g,\rm US} - \tau_{g,in})/\tau_{g,in}$ (where subscripts "US" and "in" indicate the values obtained at the same temperature with and without USL respectively) are listed in Table IV;
(iii) $\Delta n_{\rm id}$ and $\varepsilon_{\tau g}$ vary with $W_{\rm US}$ enhancement, whereas $T_{\rm id}$ and $E_{\tau g}$ values practically do not depend on US intensity;
(iv) USL leads to the increase in both $T_{\rm id}$ and $E_{\tau g}$ in γ–irradiated samples (see Fig. 3(b) and Fig. 4(b)), but this effect is not observed in non–irradiated and neutron–irradiated samples (see Fig. 3(a) and Fig. 4(a));
(v) $\Delta n_{\rm id}$ and $\varepsilon_{\tau g}$ have opposite signs for non–irradiated and irradiated samples (for SCg6 not in the whole temperature range);
(vi) ideality factor is varied by USL more effectively in the irradiated samples.

For the purpose of our analysis, it is important to dis-

TABLE III. Characteristics of temperature dependences of n^+–p–Si structure parameters.

Sample	USL	$T_{\rm id}$ (K)	$E_{\tau g}$ (eV)	$R_{293,\rm Al}$ (kΩ)	$\sigma_{\rm dis}$ (10^4 K/Ω)
iSC	non	330 ± 30	0.24 ± 0.01	27 ± 3	41 ± 4
	Ui–1	310 ± 30	0.24 ± 0.01	27 ± 3	50 ± 4
	Ui–2	360 ± 30	0.24 ± 0.01	26 ± 3	58 ± 4
nSC	non	1610 ± 70	0.45 ± 0.02	2.2 ± 0.4	65 ± 7
	Un–1	1600 ± 70	0.44 ± 0.02	2.3 ± 0.4	95 ± 10
	Un–2	1680 ± 70	0.44 ± 0.02	2.2 ± 0.4	130 ± 10
g6SC	non	610 ± 40	0.28 ± 0.01	0.7 ± 0.1	19 ± 2
	Ug6–2	1080 ± 50	0.33 ± 0.02	0.8 ± 0.1	24 ± 2
g7SC	non	770 ± 50	0.29 ± 0.01	0.41 ± 0.06	26 ± 3
	Ug7–1	1260 ± 60	0.34 ± 0.02	0.39 ± 0.06	45 ± 4
	Ug7–2	1270 ± 60	0.35 ± 0.02	0.38 ± 0.06	55 ± 4

TABLE IV. Acoustically induced change of n^+-p–Si structure parameters (at 330 K).

Sample	USL	$\Delta n_{\rm id}$ (±0.01)	$\varepsilon_{\tau g}$ (±5%)	$\varepsilon_{\tau n}$ (±0.2)	$\varepsilon_{\sigma \rm dis}$ (±10%)
iSC	Ui–1	0.02	-14	0.7	20
	Ui–2	0.03	-17	1.4	40
nSC	Un–1	-0.13	5	1.5	50
	Un–2	-0.26	13	3.0	100
g6SC	Ug6–2	-0.15	2	2.3	30
g7SC	Ug7–1	-0.26	49	0.9	70
	Ug7–2	-0.36	70	1.9	110

cuss the recombination mechanism in SCR of the investigated samples. According to classical SRH theory, the ideality factor must be smaller than 2, and τ_g temperature dependence is expected[50,51] to be described by the relation $\tau_g \simeq 2\,\tau_n \sqrt{\sigma_n/\sigma_p} \cosh\left[(E_t - E_i)/kT\right]$ (where σ_n, σ_p, and E_t are the electron and hole capture cross sections (CCSs) and the energy level of the recombination center, E_i is the intrinsic energy level). In our case, $n_{\rm id}$ is greater than 2, and τ_g increases with temperature. Therefore, SRH theory cannot be applied in our case. Several attempts to account for large $n_{\rm id}$ value have been made by using different models.[52–55] However, all the observed features of SCR recombination (large ideality factor, independence on light intensity, dependence on temperature as well as short carrier lifetime) can be explained by the model of coupled defect level recombination (CDLR)[40,41] only. This mechanism provides a rapid direct charge transfer between defect levels. The phenomenon was first observed experimentally,[56,57] after which it was recruited to explain the process in semiconductor diodes.[40,41,58]

According to CDLR model, the recombination is the result of carrier exchange between two defect levels and crystal bands. In particular, it is supposed[41] that the recombination rate is dominant at the sites where acceptor–like defect is coupled with donor-like defect. In a simplified case, when there is no carrier exchange between the donor level $E_t^{\rm D}$ and valence band, as well as between the acceptor level $E_t^{\rm A}$ and conduction band, the recombination rate R can be expressed[40] as

$$R = \frac{R_{12} - \sqrt{R_{12}^2 - 4\tau_n^{\rm D}\tau_p^{\rm A}(np - n_i^2)(1-\epsilon)}}{2\tau_n^{\rm D}\tau_p^{\rm A}(1-\epsilon)}\,, \qquad (8)$$

$$R_{12} = \frac{(n+n_{\rm D})(p+p_{\rm A})}{R_{\rm DA}} + \tau_n^{\rm D}(p+p_{\rm D}) + \tau_p^{\rm A}(n+n_{\rm A}), \qquad (9)$$

$$\tau_n^{\rm D} = (N_{\rm D}\,\sigma_n^{\rm D}\,\upsilon_{{\rm th},n})^{-1}, \quad \tau_p^{\rm A} = (N_{\rm A}\,\sigma_p^{\rm A}\,\upsilon_{{\rm th},p})^{-1}, \qquad (10)$$

where $R_{\rm DA}$ is the coupling parameter, $N_{\rm D}$ and $N_{\rm A}$ are the densities of donor and acceptor–like defects, $\sigma_n^{\rm D}$ and $\sigma_p^{\rm A}$ are electron CCS of donor and hole CCS of acceptor, $\upsilon_{{\rm th},n}$ and $\upsilon_{{\rm th},p}$ are the thermal electron and hole velocities, $n_{\rm D,A}$, $p_{\rm D,A}$, and ϵ depend on $E_t^{\rm D}$, $E_t^{\rm A}$, and level degeneracy factors. Since $\tau_g \propto R^{-1}$, the last three values are expected to provide a thermoactivated behavior of SCR lifetime. Unfortunately, the equation does not account for the functional relation between I–V characteristics parameters and attributes of defects taking part in CDLR.

According to Steingrube *et al.*[41], CCS for defect in a pair differs from that for an isolated defect and depends on the distance r between donor and acceptor:

$$\sigma_{n,p}^{\rm D,A}(r) = C_{n,p}^{\rm D,A}\, r^2\,, \qquad (11)$$

where $C_n^{\rm D}$ and $C_p^{\rm A}$ are constant values. $R_{\rm DA}$ is proportional to the overlap integral of the defects wave functions as well. If both defects are characterized by H–like radial–symmetric wave function, and equal Bohr radius a_0, the following expression can be used:[41]

$$R_{\rm DA}(r) \propto N_{\rm D} N_{\rm A} \left[1 + \frac{r}{a_0} + \frac{1}{3}\left(\frac{r}{a_0}\right)^2\right] e^{-r/a_0}\,. \qquad (12)$$

In our opinion, the observed reversible AI modifications of $n_{\rm id}$ and τ_g are induced by donor–acceptor distance alteration in the samples under USL. In fact, according to the data,[21,22] the force acting on a point defect during USL can be expressed as

$$F_d = \chi\,\Delta\Omega_d \frac{\partial \xi(z,t)}{\partial z}\,, \qquad (13)$$

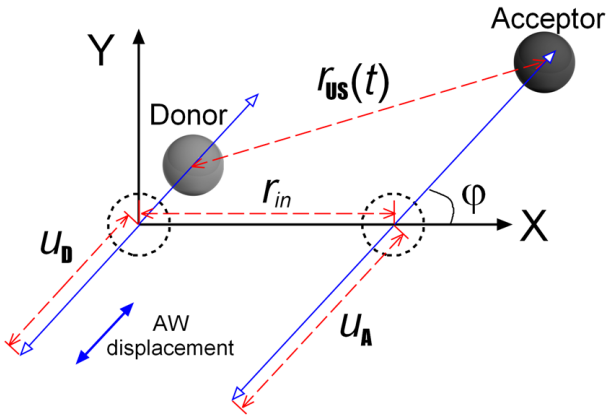

FIG. 5. Model of CDLR center behavior under US action.

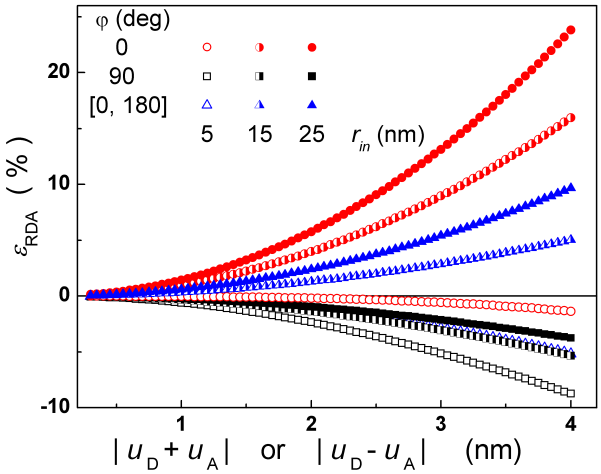

FIG. 6. Simulated dependencies of AI changes of coupling parameter on the vibration amplitudes. Axis $|u_D - u_A|$ corresponds to $\delta = 0°$ case, whereas axis $|u_D + u_A|$ corresponds to $\delta = 180°$ case. The parameters are set to $a_0 = 3.23$ nm, $r_{in} = 5$ nm (open marks), 15 nm (semi–filled marks), and 25 nm (filled marks), $\varphi = 0°$ (circles), 90° (squares). Triangles correspond to mean ε_{RDA} value for $[0° \div 180°]$ φ range.

where χ is the bulk elasticity modulus, $\Delta\Omega_d$ is the crystal volume change per defect, ξ is the crystal lattice deformation, and AW propagates along z axis, $\partial\xi(z,t)/\partial z \propto \xi_{US}$. $\Delta\Omega_d > 0$ for the interstitial atoms and substitutional impurities with ionic radius exceeding the ionic radius of matrix atoms, whereas for the vacancies and substitutional impurities whose ionic radius is smaller than that of matrix atoms $\Delta\Omega_d < 0$. Therefore, a point defect vibrates under USL, so oscillation amplitude and phase are determined by both the defect character and AW intensity.

The simplest model, which is shown in Fig. 5, gives the following qualitative conclusion. Initially, donor and acceptor are separated by the distance r_{in}, and axis X is drawn through the point defect initial positions. Under USL, the defects would vibrate with amplitudes u_D and u_A. The vibration axis coincides with AW displacement direction and forms angle φ with X–axis. Depending on ξ_{US}, defect elastic strain ($\Delta\Omega_d^D$ and $\Delta\Omega_d^A$) and defect coupling the defect vibration amplitudes can have different values. The donor–acceptor distance in the sample under USL r_{US}, according to the model, depends on time t:

$$r_{US}(t) = \left\{[r_{in} + u_A\cos(\omega_{US}t + \delta) - u_D\cos(\omega_{US}t)]^2\cos^2\varphi + [u_A\cos(\omega_{US}t + \delta) - u_D\cos(\omega_{US}t)]^2\sin^2\varphi\right\}^{0.5}, \quad (14)$$

where ω_{US} is the US cyclic frequency and δ is the phase shift between donor and acceptor vibration.

We use Eqs. (11)–(12) to estimate AI relative changes of CCS $\varepsilon_\sigma = [\sigma_{US} - \sigma(r_{in})]/\sigma(r_{in})$ and coupling parameters $\varepsilon_{RDA} = [R_{DA,US} - R_{DA}(r_{in})]/R_{DA}(r_{in})$, where σ_{US} and $R_{DA,US}$ are averaged over the AW period T_{US}:

$$\sigma_{US} = \frac{1}{T_{US}}\int_0^{T_{US}}\sigma(r_{US}(t))dt\,,\; R_{DA,US} = \frac{1}{T_{US}}\int_0^{T_{US}}R_{DA}(r_{US}(t))dt\,.$$

In this estimation, the relaxation time in the CDLR subsystem is assumed to be considerably shorter than T_{US}, and we apply the previously used[41] value $a_0 = 3.23$ nm.

In addition, the chosen u_D and u_A values are commensurate with u_{US}. However, it should be taken into account, that the displacement of the point defect without covalent bond could exceed a matrix atom displacement. Finally, no US absorption by defect is assumed. In this simple case, δ is equal to 0° if $(\Delta\Omega_d^D \cdot \Delta\Omega_d^A) > 0$, or to 180° if $(\Delta\Omega_d^D \cdot \Delta\Omega_d^A) < 0$. In addition, ε_{RDA} exclusively depends on $|u_D - u_A|$ (in $\delta = 0°$ case) or $|u_D + u_A|$ (in $\delta = 180°$ case). Moreover, these dependences are identical in both cases. The typical results of simulation of coupling parameter changes are shown in Fig. 6.

Relative changes of CCS depends on oscillation amplitudes with similar features and does not depend on φ:

$$\varepsilon_\sigma = (u_D \pm u_A)^2/2\,r_{in}^2 = K_{US}^{DA}W_{US}\,, \quad (15)$$

where "+" and "−" correspond to $\delta = 180°$ and $\delta = 0°$ respectively, K_{US}^{DA} characterizes defect couple–ultrasound interaction and depends on properties defects as well as crystal matrix. Eq. (15) takes into account that $u_D, u_A \propto \xi_{US} \propto \sqrt{W_{US}}$.

It is worth keeping in mind that CDLR current flows locally in the locations of extended defects.[41,58] At the same time, the dislocations are often located perpendicularly to $p-n$ junction plane in the SCR region, and the investigated samples are not exception (see Section III C). If coupled defects and dislocations are close to each other, then the dislocations with edge component should affect the pair spatial orientation. Thus, the axis of donor–acceptor pair with $(\Delta\Omega_d^D \cdot \Delta\Omega_d^A > 0)$ should be predominantly parallel to dislocation line, whereas the axis of a pair of coupled defects with $(\Delta\Omega_d^D \cdot \Delta\Omega_d^A < 0)$ should make a right angle with dislocation line. As AW displacement is parallel to the $p-n$ junction plane, the cases of most

exciting interest are the following:
$\delta = 0°$, $\varphi = 90°$ ($\Delta\Omega_d^{\mathtt{D}} \cdot \Delta\Omega_d^{\mathtt{A}} > 0$ case);
$\delta = 180°$, $\varphi \in [0° \div 180°]$ ($\Delta\Omega_d^{\mathtt{D}} \cdot \Delta\Omega_d^{\mathtt{A}} < 0$ case).
In other words, all curves in Fig. 6 can be realized if defect volume relaxation of donor–like defect has the sign opposite to that of acceptor–like defect. Moreover, only squares should to be under consideration in case of $\Delta\Omega_d^{\mathtt{D}} \cdot \Delta\Omega_d^{\mathtt{A}} > 0$.

Taking into account the experimental results and the estimation suggested by our model:
(i) $E_{\tau g}$ and $T_{\rm id}$ are mainly determined by couple component energy levels. The alteration of $E_{\tau g}$ and $T_{\rm id}$ for nSC, g6SC, and g7SC in comparison with iSC testifies to the change of defect (donor, acceptor, or both) which take part in CDLR after irradiation. g6SC defects are coincident to g7SC defects and differ from neutron–irradiated sample defects.
(ii) USL causes donor–acceptor distance change and results in ε_σ and $\varepsilon_{\mathtt{RDA}}$, which increase with $W_{\mathtt{US}}$.
(iii) Acoustically induced $E_{\tau g}$ (and $T_{\rm id}$) modification, which is observed in g6SC and g7SC only, testifies to the rebuilding of γ–induced RD, i.e., γ–induced RD is congurationally bistable (or metastable) and transforms from ground state under US action. Similar AI defect variations were also reported previously.[3,5,32,59]
(iv) ε_σ sign is immutable — see Eq. (15), whereas $\varepsilon_{\mathtt{RDA}}$ sign can vary for the pair with opposite relaxation volume component (see Fig. 6). Therefore, change of $\Delta n_{\rm id}$ and $\varepsilon_{\tau g}$ sign is the evidence of transformation from ($\Delta\Omega_d^{\mathtt{D}} \cdot \Delta\Omega_d^{\mathtt{A}} > 0$) to ($\Delta\Omega_d^{\mathtt{D}} \cdot \Delta\Omega_d^{\mathtt{A}} < 0$) after irradiation. The transformation is confirmed by the enhanced efficiency of US action on defects in irradiated samples. In fact, in the case of ($\Delta\Omega_d^{\mathtt{D}} \cdot \Delta\Omega_d^{\mathtt{A}} < 0$) the US efficiency is determined by the sum of pair component displacements, whereas in the contrary case — by their difference. In our opinion, both donor and acceptor are defects of interstitial–type in non–irradiated sample, and one of pair components is a defect of vacancy–type in irradiated samples. The defect configurations are discussed below, in Section III D.

B. Quasi–neutral region

Base lifetime describes the processes which occur in the quasi–neutral region of p-n–structure. Fig. 7 shows τ_n behaviour in the explored temperature range. As expected, minority carrier lifetime increases as the temperature grows, and at 320 K, τ_n values comprise $2 \div 5$ μs for different samples, which correspond to $80 \div 130$ μm range of diffusion lengths. In our opinion, the observed τ_n dispersion is caused not by irradiation, but rather deals with sample–ancestor wafer inhomogeneity, which is often the case.[60,61]

In fact, the irradiation induced lifetime reduction is described by the Messenger-Spratt equation:[48]

$$\tau_n^{-1} = \tau_{n0}^{-1} + K_\tau \Psi \,, \qquad (16)$$

TABLE V. Measured and estimated base lifetime parameters.

Sample	$\tau_{n,in}^{-1}$ (320 K) (10^5 s^{-1})	K_τ (cm^2/s)	$K_\tau \times \Psi$ (10^4 s^{-1})	$K_{\mathtt{US}}^{\mathtt{eff}}$ (cm^2/W)
iSC	2.9	—	—	3.5
nSC	4.7	10^{-7}(Ref. 33) $2{\cdot}10^{-7}$(Ref. 62)	$4 \div 8$	7.1
g6SC	1.8	$5{\cdot}10^{-12}$	0.8	6.0
g7SC	2.8	(Refs. 33, 63)	8	5.2

where τ_{n0} is the minority carrier lifetime in non–irradiated sample and K_τ is a lifetime damage constant. The known K_τ values and estimated changes of reciprocal base lifetime $K_\tau\Psi$ are shown in Table V. As seen from the table, the estimated value of radiation–induced τ_n^{-1} change comprises $(8 \div 17)$, 4, and 29 % of the values measured for samples nSC, g6SC and g7SC, respectively, so this cannot explain the dispersion observed experimentally. At the same time, the calculated lifetime changes $K_\tau\Psi$ are in quite good agreement with the changes expected from RDs production — see Section III D.

Base lifetime can be expressed as follows:[64]

$$\tau_n^{-1} = \tau_{\mathtt{bb}}^{-1} + \tau_{\mathtt{CE\,Auger}}^{-1} + \tau_{\mathtt{SRH}}^{-1} \,, \qquad (17)$$

where $\tau_{\mathtt{bb}}$, $\tau_{\mathtt{CE\,Auger}}$, $\tau_{\mathtt{SRH}}$ are the lifetimes of band–to–band recombination, Coloumb–enhanced Auger recombination, and SRH recombination, respectively. The calculation shows that $\tau_{\mathtt{bb}}^{-1} = 14$ s^{-1}, $\tau_{\mathtt{CE\,Auger}}^{-1} = 6$ s^{-1}. Therefore, band–to–band recombination and Auger recombination can be neglected. In case of low injection level and single recombination centre, SRH lifetime is described by Eq. (10). If there are several centers of recombination, the following equation should be applied

$$\tau_n^{-1} = \sum_i^{M_d} \tau_{n,i}^{-1} = \sum_i^{M_d} N_{d,i}, \sigma_{n,i}\, \upsilon_{{\rm th},n} \,, \qquad (18)$$

where M_d is the total number of centers, $\tau_{n,i}$ characterizes lifetime due to recombination by i–th defect, $N_{d,i}$ and $\sigma_{n,i}$ are the concentration and electron CCS of i–th defect, respectively.

Fig. 7 shows that USL results in τ_n decrease. Relative AI changes of reciprocal base lifetime $\varepsilon_{\tau n} = (\tau_{n,in} - \tau_{n,\mathtt{US}})/\tau_{n,\mathtt{US}}$ are listed in Table IV. As AI changes are reversible, the lifetime alteration, in our opinion, deals with the increase of σ_n under US action. Following the empirical relation proposed by Ref. 65, we assume that Eq. (11) is valid for a complex point defect as well. In this case, however, r is the distance which separates the components of a complex. According to the model suggested in Section III A, USL leads to r variation and σ_n change in line with Eq. (15). In case of CDLR, AI change of capture cross section of donor (or/and acceptor) is supplemental to the variation of both the coupling parameter and the couple distance, but only CCS change determines the AI variation of base lifetime.

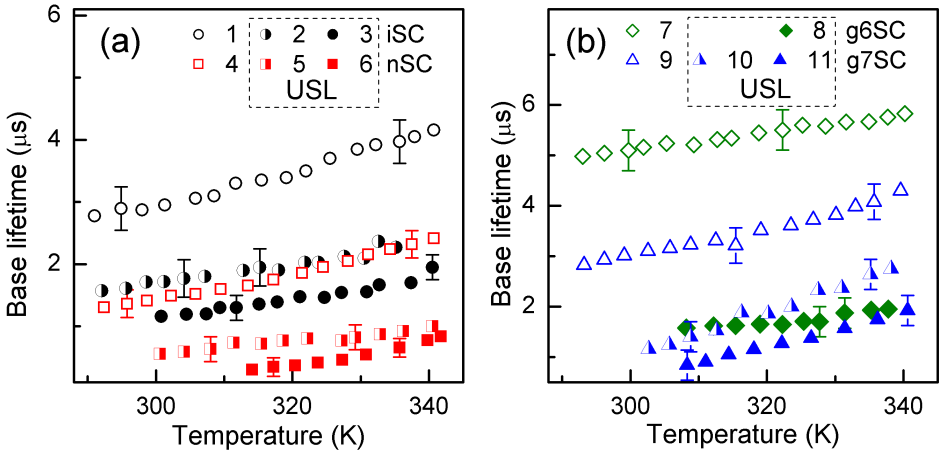

FIG. 7. Temperature dependences of base lifetime for non–irradiated (curves 1–3, circles), neutron–irradiated (4–6, squares) and γ–irradiated (7–11, diamonds and triangles) samples. The curves 1, 4, 7 and 9 (open marks) are obtained without USL, curves 2, 3, 5, 6, 8, 10, and 11 correspond to Ui–1, Ui–2, Un–1, Un–2, Ug6–2, Ug7–1, and Ug7–2 respectively.

However, not every defect effectively takes part in AID. If $M_d^{\mathtt{AA}}$ and $M_d^{\mathtt{nonAA}}$ are the total numbers of acoustically active (AA) and non–acoustically active (non–AA) centers, Eq (18) for τ_n^{-1} under USL and without it takes the following shape

$$\tau_{n,in}^{-1} = \sum_j^{M_d^{\mathtt{AA}}} N_{d,j}, \sigma_{n,j}^{in}\, \upsilon_{\mathrm{th},n} + \sum_l^{M_d^{\mathtt{nonAA}}} N_{d,l}, \sigma_{n,l}\, \upsilon_{\mathrm{th},n}\,,$$

$$\tau_{n,\mathtt{US}}^{-1} = \sum_j^{M_d^{\mathtt{AA}}} N_{d,j}, \sigma_{n,j}^{\mathtt{US}}\, \upsilon_{\mathrm{th},n} + \sum_l^{M_d^{\mathtt{nonAA}}} N_{d,l}, \sigma_{n,l}\, \upsilon_{\mathrm{th},n}\,.$$

By using Eq (15), $\varepsilon_{\tau n}$ is transformed as follows

$$\varepsilon_{\tau n} = K_{\mathtt{US}}^{\mathtt{eff}} W_{\mathtt{US}}\,, \tag{19}$$

where $K_{\mathtt{US}}^{\mathtt{eff}}$ characterizes ADI in the sample and depends on the concentration of both AA and non–AA centers

$$K_{\mathtt{US}}^{\mathtt{eff}} = \sum_j^{M_d^{\mathtt{AA}}} \frac{\tau_{n,in}}{\tau_{n,j,in}} K_{\mathtt{US,j}}\,, \tag{20}$$

$K_{\mathtt{US,j}}$ deals with j–th defect–ultrasound interaction.

The obtained dependences of $\varepsilon_{\tau n}$ vs $W_{\mathtt{US}}$ are shown in Fig. 8. The linearity of these dependences prove the correctness of our assumptions. The obtained $K_{\mathtt{US}}^{\mathtt{eff}}$ values are listed in Table V. The non–monotonic $K_{\mathtt{US}}^{\mathtt{eff}}$ alteration with γ dose is discussed in Section III D.

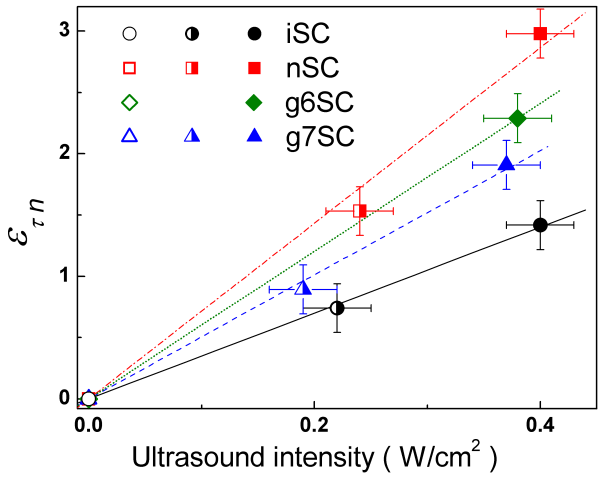

FIG. 8. Dependences of base lifetime relative change on US intensity for non–irradiated (circles), neutron–irradiated (squares), and γ–irradiated (triangles and diamonds) samples. Lines are the fitted curves using Eq. (19).

C. Shunt resistance

Fig. 9 shows the shunt resistance over the explored temperature range. As seen from the figure, the irradiation results in R_{sh} decrease. Also, the R_{sh} temperature dependence changes after γ–irradiation. In particular the shunt resistance decreases with the temperature growth in iSC and nSC, whereas in g6SC and g7SC the increase of R_{sh} vs T is close to linear at the vicinity of 293 K. It should be noted that R_{sh} axis is logarithmic in Fig. 9(a) and linear in Fig. 9(b).

The shunt resistance is known[66] to occur in p–n structure due to several non–mechanical reasons. It can be caused by aluminum particles, macroscopic Si_3N_4 inclusions or inversion layers at precipitates. In the course of firing, Al particle can penetrate into the sample creating p^+–doped region around itself, which compensates the emitter and remains in ohmic contact with the base. Inversion layers and Si_3N_4 inclusions occur mainly in multicrystalline silicon cells[66] and cannot cause shunt resistance in the investigated samples. Dislocations, however, which intersect the junction, are generally held re-

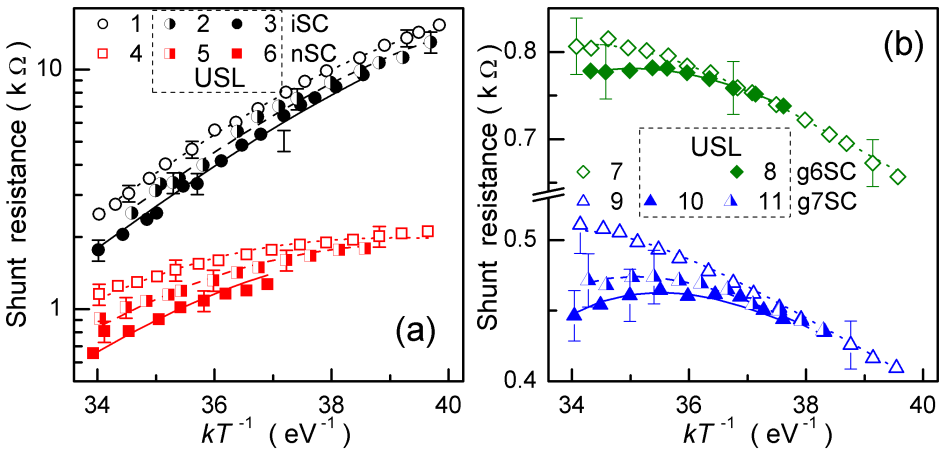

FIG. 9. Temperature dependences of shunt resistance for non–irradiated (curves 1–3, circles), neutron–irradiated (4–6, squares) and γ–irradiated (7–11, diamonds and triangles) samples. The curves 1, 4, 7 and 9 (open marks) are obtained without USL, curves 2, 3, 5, 6, 8, 10, and 11 correspond to Ui–1, Ui–2, Un–1, Un–2, Ug6–2, Ug7–1, and Ug7–2 respectively. The marks are the experimental results, the lines are the fitted curves using Eq. (21)-(23).

sponsible as a possible source of ohmic current.[66–68] In our opinion, both aluminum particles and dislocations are present in the investigated structures, so the overall shunt resistance can be expressed as

$$R_{sh}^{-1} = R_{sh,\mathrm{Al}}^{-1} + R_{sh,\mathrm{dis}}^{-1}\,, \qquad (21)$$

where $R_{sh,\mathrm{Al}}$ and $R_{sh,\mathrm{dis}}$ deal with aluminum particles and dislocations, respectively. The linear temperature dependence of metal particles $R_{sh,\mathrm{Al}}$ is suggested:

$$R_{sh,\mathrm{Al}} = R_{293,\mathrm{Al}}[1 + \alpha(T - 293)]\,, \qquad (22)$$

where $R_{293,\mathrm{Al}}$ is the shunt resistance at 293 K and α is the resistance temperature coefficient.

According to the model of dislocation–induced impedance of photovoltaic detector suggested by Gopal and Gupta,[42,43] $R_{sh,\mathrm{dis}}$ can be given by:

$$R_{sh,\mathrm{dis}} = \frac{T}{\sigma_{\mathrm{dis}}}\left[\cosh\left(\frac{E_{\mathrm{dis}} - E_i}{kT}\right) + \cosh\left(\frac{U_s}{kT}\right)\right], \qquad (23)$$

with

$$\sigma_{\mathrm{dis}} = \rho_{\mathrm{dis}} A q^2 A_{\mathrm{dis}} \sqrt{K_n K_p}\, N_{\mathrm{dis}}(n_p + p_p)/k\,, \qquad (24)$$

where E_{dis} is the energy level which significantly contributes to the dislocation recombination current, U_s is the potential at the surface of the dislocation core, ρ_{dis} and A_{dis} are the dislocation density and surface area, respectively, K_n and K_p are the probabilities for electrons and holes capture by the dislocation states, N_{dis} is the density of surface states at each dislocation. Eq. (23) is true for simplified case of $K_p = K_n$.

The resistance temperature coefficient was estimated from data on g7SC. The obtained value $8.3 \cdot 10^{-3}$ K^{-1} is not far from resistance temperature coefficient of bulk Al ($4.3 \cdot 10^{-3}$ K^{-1}). To fit the experimental data for R_{sh}, we used Eqs. (21)–(23). As the fitting parameters, $R_{293,\mathrm{Al}}$, $(E_{\mathrm{dis}} - E_i)$, U_s, and σ_{dis} were taken. It has been found that the experimental data are in good agreement with the fitting curves (see Fig. 9) for values $(E_{\mathrm{dis}} - E_i) = (0.46 \pm 0.02)$ eV and $U_s = (5 \pm 4) \times 10^{-8}$ eV, which were independent of irradiation and USL. The obtained value of $(E_{\mathrm{dis}} - E_i)$ corresponds to the carrier activation energy 0.10 ± 0.02 eV and is comparable with the activation energy of dislocation levels 0.08 eV, which was earlier reported[69–73] in Cz–Si:B as well.[69–71]

The obtained values of $R_{293,\mathrm{Al}}$ and σ_{dis} are given in Table III. $R_{293,\mathrm{Al}}$ does not depend on USL and increases as the irradiation level. In our opinion, $R_{sh,\mathrm{dis}}$ is smaller than $R_{sh,\mathrm{Al}}$ in iSC. The irradiation facilitates the formation of vacancies as well as Al diffusion out of the electrodes. As a consequence, the number of Al particles grow, $R_{sh,\mathrm{Al}}$ decreases and becomes the key factor contributing in the overall shunt resistance. Al diffuses more effectively in the samples exposed to γ–radiation due to a more uniform distribution of irradiation–induced single vacancies.

Dispersion of σ_{dis} correlate with dispersion of τ_n over the samples set. Hence, σ_{dis} dispersion deals with wafer inhomogeneity too. USL causes σ_{dis} increase, relative AI changes $\varepsilon_{\sigma\mathrm{dis}} = (\sigma_{\mathrm{dis,US}} - \sigma_{\mathrm{dis},in})/\sigma_{\mathrm{dis},in}$ are shown in Table IV. In our opinion this is caused by an A_{dis} augmentation. Namely, the dislocation core atom displacement is normal to the current direction. As the result, the carriers are captured by dislocation levels from enlarged volume. Therefore, the effective surface area increases and $R_{sh,\mathrm{dis}}$ decreases due to US action.

D. Defect type speculation

Lifetime killers in boron–doped Czochralski–grown Si are boron–oxygen related (BO) defects,[74,75] iron–boron

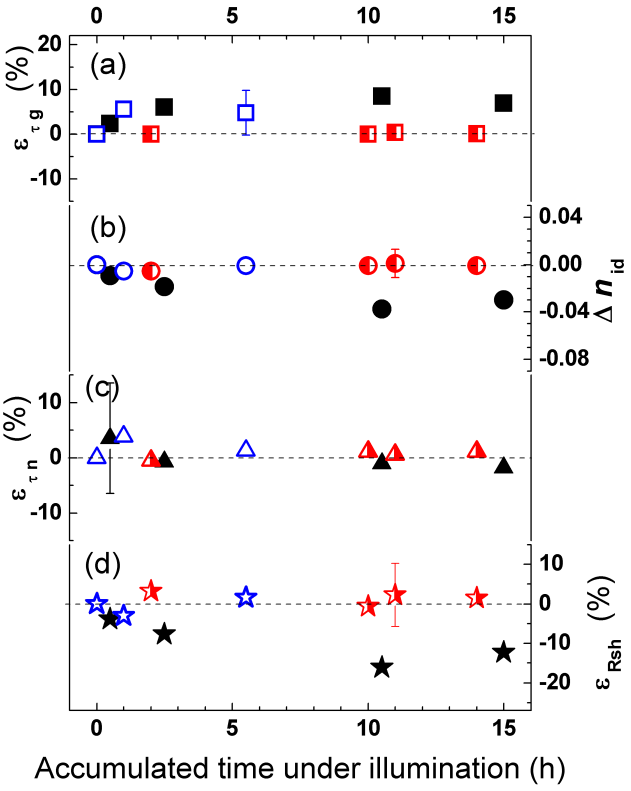

FIG. 10. Permanent changes of SCR lifetime (a, squares), ideality factor (b, circles), base lifetime (c, triangles), and shunt resistance (d, asterisks) versus accumulated illumination time. Sample iSC, $T = 295$ K. Filled, semi–filled and open marks correspond to sample before annealing, after first 10 min 200 °C annealing, and after second 10 min 200 °C annealing, respectively.

pairs[64,76,77] (or another Fe–related trap in the n^+p–junctions[78,79]), and oxide precipitates.[60,61,64,80–82] The first two defects are sensitive to intensive illumination at room temperature. To determine the major recombination center in the investigated samples the following experimental procedure was used. The non-irradiated sample was light soaked under illumination by halogen lamp (2 Suns) at approximately 305 K. The illumination time varied from 1 h to 8 h. After illumination was terminated, the sample was exposed to room temperature in the darkness. Over 5 h period, I–V characteristics were measured at room temperature with the interval 10–15 min in order to determine the kinetics of the parameters. To estimate the permanent light–induced change, the measurements of I–V characteristics were performed in 48 h after illumination. After the total time under illumination ran up to 15 h, the iSC was annealed at 200 °C for 10 min in darkness, after which the measurements were carried out at room temperature. Then the illumination and measurements were repeated.

Intensive light is known[74,75] to cause permanent transformation of BO defects and considerable decrease of minority–carrier lifetime (as low as 10 % of initial value

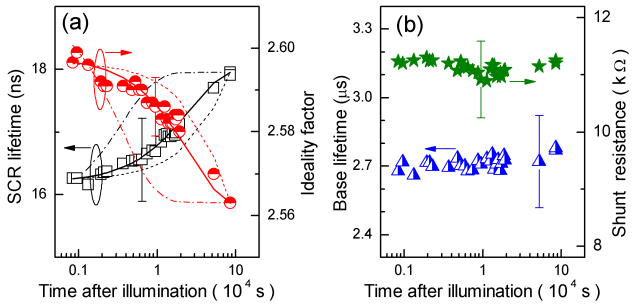

FIG. 11. SCR lifetime (a, squares, left axis), ideality factor (a, circles, right axis), base lifetime (b, triangles, left axis), and shunt resistance (b, asterisks, right axis) as a function of time since illumination stoping. Sample iSC, $T = 295$ K. Lines are calculated by using Eqs.(25)–(26) and $E_{\mathrm{D,Fe}} = 0.63$ eV (dash–dotted lines), 0.68 eV (solid lines), and 0.73 eV (dashed lines).

at long term illumination). Annealing at 200 °C for 10 min in the darkness results in both recovery of state and readiness to light–induced degradation of BO defects. Fig. 10 shows the changes of structure parameters in comparison with those prior to illumination. As seen from the figure, illumination does not result in considerable permanent change of τ_g, τ_n, n_{id} before as well as after annealing. Therefore, BO influence on recombination can be neglected in both SCR and the base.

At the same time, the vast majority of impurity iron exists in iron–boron pairs. Fe_iB_s can be readily dissociated under intense illumination to release interstitial iron, which results in lifetime changes. In the darkness, Fe_iB_s is repaired and Fe_i concentration decreases according to[64,83]

$$N_{Fe}(t) = (N_{Fe,0} - N_{Fe,eq}) \exp\left[-\frac{t}{\tau_{\mathrm{rep}}}\right] + N_{Fe,eq}\,, \quad (25)$$

where $N_{Fe,0}$ is the concentration immediately after illumination, and $N_{Fe,eq}$ is the equilibrium concentration which remains for a long time after dissociation; the characteristic time of repairing τ_{rep} depends on doping level

$$\tau_{\mathrm{rep}} = 770 \cdot p_p^{-2/3} \exp\left(\frac{E_{\mathrm{D,Fe}}}{kT}\right)\,, \quad (26)$$

$E_{\mathrm{D,Fe}} = 0.68$ eV is the activation energy of Fe_i diffusion.

It was found that n_{id} increased (by about 0.03) and τ_g decreased (by about 10 %) immediately after illumination — see Fig. 11(a). These changes vanished gradually. We supposed that τ_g and n_{id} evolutions could be described by expressions similar to Eq. (25). The obtained Eq. (26) was used to calculate characteristic time, and the fitting lines are presented on Fig. 11(a). The fittings with $E_{\mathrm{D,Fe}} = 0.68$ eV are in good agreement with the experimental data. Hence, it is evident that iron–boron pairs take part in SCR recombination. At the same time, electron and hole CCS of Fe_i are 1.7 and 0.04 times[64] as much as those of Fe_iB_s. A small τ_g alteration (by about 10 %), caused by light is the evidence of the supporting role

of iron–boron pair in SCR recombination. Furthermore, since τ_n does not depend on illumination (see Fig. 11(b)), Fe_iB_s does not influence on base lifetime.

Thus, a conclusion can be made that oxide precipitates are number one agents in SCR and base recombinations. According to Murphy *et al.*[80,81], there exist at least two independent oxide precipitate related defects. These defects have $\sigma_n/\sigma_p = 157$ and $\sigma_p/\sigma_n = 1200$ respectively,[81] which is suitable for CDLR. These facts allow us to conclude that the defect responsible for AI phenomena in iSC is mainly oxide precipitate.

In foreseeing RD type, it is worth keeping in mind doping level, oxygen concentration and irradiation dose. In our case (Czochralski, oxygen–rich, $\sim 7\cdot10^{17}$ cm^{-3}, p–Si with boron concentration $\sim 10^{15}$ cm^{-3} and low dose) it is expected that C_iO_i, vacancy clusters V_n (divacancy V_2, trivacancy V_3, ...) and VO_i are produced mainly by neutron irradiation[84–86] while C_iO_i and VO_i — by γ–rays.[86–89] The RD concentration $N_{t,\mathrm{RD}}$ linearly depends on dose, the known introduction rate for neutron η_n and gamma η_γ irradiation in Cz–Si are shown in Table VI. The expected values of $N_{t,\mathrm{RD}}$ for the investigated samples are listed in Table VI as well.

The other defects that can be created by irradiation in silicon are I_p–center, bistable donor (BD), B_iO_i and C_iC_s. At the same time, I_p–center and BD are characterized by small introduction rate. For example, the expected[85,93] concentration of BD is only $(1 \div 2)\cdot 10^{10}$ cm^{-3} in nSC and g7SC. The lack of B_iO_i in the investigated samples deals with low boron concentration[94]. The formation of C_iC_s is suppressed in oxygen–rich crystal[84,87,88] and, what is more, C_iC_s is not an active recombination center.[95]

The influence of RD on base lifetime could be estimated by Eq. (18) taking into account the fact that VO_i is a recombination center which is not active in p–Si.[63,96–99] The estimated $\tau_{n,\mathrm{RD}}$ for C_iO_i, V_2, and V_3 are shown in Table VI. As seen from the table, τ_n is effected mainly by C_iO_i in γ–irradiated samples and by vacancy clusters in nSC. It should be noted, that nSC, g6SC, g7SC sums of $\tau^{-1}_{n,\mathrm{RD}}$ are in quite good agreement with $(K_\tau\cdot\Psi)$ values.

We shall now consider $K_{\mathrm{US}}^{\mathrm{eff}}$ for non–irradiated sample assuming $M_d^{\mathrm{AA}} = 1$ and $M_d^{\mathrm{nonAA}} = 1$. We shall also assume that US interactions with C_iO_i and V_n are described by $K_{\mathrm{US}}^{\mathrm{CO}}$ and $K_{\mathrm{US}}^{\mathrm{V}}$, respectively. Then Eq. (20) gives the following expression for $K_{\mathrm{US}}^{\mathrm{eff}}$ in iSC and irradiated samples:

$$K_{\mathrm{US}}^{\mathrm{eff}} = K_{\mathrm{US}}^{\mathrm{AA}}\,\tau_{n,in}/\tau_{n,in}^{\mathrm{AA}}\,,$$
$$K_{\mathrm{US}}^{\mathrm{eff}} = K_{\mathrm{US}}^{\mathrm{AA}}\tau_{n,in}/\tau_{n,in}^{\mathrm{AA}} + K_{\mathrm{US}}^{\mathrm{CO}}\tau_{n,in}/\tau_{n,\mathrm{RD}}^{\mathrm{CO}} + K_{\mathrm{US}}^{\mathrm{V}}\tau_{n,in}/\tau_{n,\mathrm{RD}}^{\mathrm{V}}\,.$$

$\tau_{n,in}^{\mathrm{AA}}$ is the base lifetime in the sample with sole non-radiative AA defect and $K_{\mathrm{US}}^{\mathrm{AA}}$ describes ADI.

For the analysis the following two limit cases are appropriate. In the first one, non–AA defects are distributed uniformly across the wafer, and AA defects define $(\tau^{-1}_{n,in} - K_\tau\cdot\Psi)$ values in different samples. In the second one, a non–AA defect distribution is not uniform, and $\tau_{n,in}^{\mathrm{AA}}$ is identical for iSC, nSC, g6SC, and g7SC. However, in the first case (as well as in case of $M_d^{\mathrm{nonAA}} = 0$), the experimental values of $K_{\mathrm{US}}^{\mathrm{eff}}$ lead to unreal (negative) values of $K_{\mathrm{US,j}}$. In the second case, Eq. (20) and the data from Tables V and VI, give the following array equations:

$$\begin{aligned}
\mathrm{iSC}:&\ 3.5 = K_{\mathrm{US}}^{\mathrm{AA}}\cdot(\tau_{n,in}^{\mathrm{AA}})^{-1}/2.9\,,\\
\mathrm{nSC}:&\ 7.1 = K_{\mathrm{US}}^{\mathrm{AA}}\cdot(\tau_{n,in}^{\mathrm{AA}})^{-1}/4.7 + 0.09\,K_{\mathrm{US}}^{\mathrm{V}} + 0.02\,K_{\mathrm{US}}^{\mathrm{CO}}\,,\\
\mathrm{g6SC}:&\ 6.0 = K_{\mathrm{US}}^{\mathrm{AA}}\cdot(\tau_{n,in}^{\mathrm{AA}})^{-1}/1.8 + 0.01\,K_{\mathrm{US}}^{\mathrm{V}} + 0.05\,K_{\mathrm{US}}^{\mathrm{CO}}\,,\\
\mathrm{g7SC}:&\ 5.2 = K_{\mathrm{US}}^{\mathrm{AA}}\cdot(\tau_{n,in}^{\mathrm{AA}})^{-1}/2.8 + 0.05\,K_{\mathrm{US}}^{\mathrm{V}} + 0.35\,K_{\mathrm{US}}^{\mathrm{CO}}\,,
\end{aligned}$$

where $(\tau_{n,in}^{\mathrm{AA}})^{-1}$ in 10^4/ s. These equations are valid for $K_{\mathrm{US}}^{\mathrm{AA}}\cdot(\tau_{n,in}^{\mathrm{AA}})^{-1} = (10\pm3)$ cm^2/W, $K_{\mathrm{US}}^{\mathrm{V}} = (42\pm15)$ cm^2/W, $K_{\mathrm{US}}^{\mathrm{CO}} = 0$. Since $(\tau_{n,in}^{\mathrm{AA}})^{-1} < 1.83$, $K_{\mathrm{US}}^{\mathrm{AA}} > 5$ cm^2/W. Thus, the observed change in base lifetime is caused by AI modification of the same defect (most likely oxide precipitates) in both non–irradiated and γ–irradiated samples. This effect is enhanced by AI alteration of divacancy in neutron–irradiated samples. In other words, C_iO_i is non–AA defect, whereas V_2 is AA defect.

In our opinion, under US action, τ_g and n_{id} in non–irradiated sample depend on modification of coupled oxide precipitate related defects. As assumed in Section III A, in irradiated samples the AA radiation defects with $\Delta\Omega_d < 0$ take part in CDLR. Divacancy is quite suitable explanation for AI influence on τ_g and n_{id} in nSC, but in γ–irradiated samples a bistable (or metastable) defect is expected. A few similar defects with $\Delta\Omega_d < 0$ are known in Si, viz VO_2,[100] V_3,[91] and VO_i.[101] VO_2 is formed after 300°C annealing of irradiated crystal, V_3 is not typical defect for $\gamma-{}^{60}$Co exposed silicon, while VO_i is largo manum produced and can take part in CDLR around n^+–p interface in g6SC and g7SC. The metastable state commonly observed at low temperature is remarkable for the large oxygen–vacancy distance and deeper energy level.[101] The volume change of entire complex is negative, whereas for the complex component $\Delta\Omega_d(\mathrm{V}) < 0$ and $\Delta\Omega_d(\mathrm{O}_i) > 0$. Hence, under assumption made, VO_i is a favorable pair for AI alteration of distance between component and therefore, can be transformed into metastable configuration by USL, which causes changes in both T_{id} and $E_{\tau g}$.

IV. CONCLUSION

The influence of ultrasound on I–V characteristics of non-irradiated silicon n^+–p–structures as well as silicon structures exposed to reactor neutrons or ^{60}Co gamma radiation have been investigated experimentally. The investigation has revealed acoustically driven reversible decrease in both the minority carrier lifetime and shunt resistance in the structure base. The effect is intensified in the irradiated structures. The analysis has shown that these effects are caused by acoustically induced increase in carrier capture coefficient for point or extended defects. It has also been found that ul-

TABLE VI. Cited and calculated defect parameters.

Defect	σ_n (10^{-15} cm^2)	η_n (cm^{-1}) Ref. 86	η_γ	$N_{t,\mathrm{RD}}(10^{11}$ cm$^{-3})$ nSC	g6SC	g7SC	$\tau^{-1}_{n,\mathrm{RD}}$ (10^4 s^{-1}) nSC	g6SC	g7SC
C_iO_i	0.7 (Ref. 87) 0.9 (Ref. 88)	1.38	$6{\cdot}10^5$ rad^{-1}cm^{-3} (Ref. 87) $4{\cdot}10^{-4}$ cm^{-1} (Ref. 88)	5.5	6	60	$0.8 \div 1$	$0.9 \div 1.1$	$9 \div 11$
V_2	3 (Ref. 87) 2 (Ref. 90)	1.21	$3{\cdot}10^4$ rad^{-1}cm^{-3} (Ref. 87)	4.8	0.3	3	$2.2 \div 3.3$	$0.1 \div 0.2$	$1 \div 2$
V_3	2.4 (Ref. 91)	0.37	—	1.5	—	—	0.7	—	—
VO_i	2.4 (Ref. 89) 4 (Ref. 92)	0.52	$7{\cdot}10^5$ rad^{-1}cm^{-3} (Ref. 87) $4{\cdot}10^{-4}$ cm^{-1} (Ref. 88)	2	$6 \div 7$	$60 \div 70$			

trasound loading leads to the reversible modification of SCR carrier lifetime and ideality factor. The changes are opposite in non–irradiated and irradiated structures. The qualitative model of the observed phenomenon, which is based on the increase in the distance between coupled defects or between complex defect components due to ultrasound action, has been suggested. It has been shown that interstitial carbon–interstitial oxygen complexes practically do not take part in acousto–defect interactions whereas divacancy in neutron– exposed structures and vacancy–interstitial oxygen pairs in γ–exposed structures can be effectively modified by applying ultrasound. Thus, ultrasound can be an effective tool for controlling silicon structure characteristics.

[1] M. Jivanescu, A. Romanyuk, and A. Stesmans, J. Appl. Phys. **107**, 114307 (2010).
[2] A. Romanyuk, P. Oelhafen, R. Kurps, and V. Melnik, Appl. Phys. Lett. **90**, 013118 (2007).
[3] I. A. Buyanova, S. S. Ostapenko, M. K. Sheinkman, and M. Murrikov, Semicond. Sci. Technol. **9**, 158 (1994).
[4] O. Korotchenkov and H. Grimmliss, Phys. Rev. B **52**, 14598 (1995).
[5] O. Y. Olikh, Semiconductors **43**, 745 (2009).
[6] S. S. Ostapenko and R. E. Bell, Journal of Applied Physics **77**, 5458 (1995).
[7] I. Ostrovskii, O. Korotchenkov, O. Olikh, A. Podolyan, R. Chupryna, and M. Torres-Cisneros, J. Opt. A: Pure Appl. Opt. **3**, S82 (2001).
[8] D. Kropman, V. Seeman, S. Dolgov, and A. Medvids, phys. stat. sol. (c) **13**, 793 (2016).
[9] N. Zaveryukhina, E. Zaveryukhina, S. Vlasov, and B. Zaveryukhin, Technical Physics Letters **34**, 241 (2008).
[10] S. A. Mirsagatov, I. B. Sapaeva, and Z. Nazarov, Inorganic Materials **51**, 1 (2015).
[11] R. Savkina, A. Smirnov, T. Kryshtab, and A. Kryvko, Mater. Sci. Semicond. Process. **37**, 179 (2015).
[12] M. Virot, R. Pflieger, E. V. Skorb, J. Ravaux, T. Zemb, and H. Mohwald, J. Phys. Chem. C **119**, 15493 (2012).
[13] O. Y. Olikh, K. V. Voytenko, R. M. Burbelo, and J. M. Olikh, Journal of Semiconductors **37**, 122002 (2016).
[14] O. Olikh, Semiconductors **45**, 798 (2011).
[15] A. Davletova and S. Z. Karazhanov, Journal of Physics and Chemistry of Solids **70**, 989 (2009).
[16] A. Davletova and S. Z. Karazhanov, Journal of Physics D: Applied Physics **41**, 165107 (2008).
[17] V. Melnik, Y. Olikh, V. Popov, B. Romanyuk, Y. Goltvyanskii, and A. Evtukh, Materials Science & Engineering, B: Solid-State Materials for Advanced Technology **124–125**, 327 (2005).
[18] O. Y. Olikh, K. V. Voytenko, and R. M. Burbelo, Journal of Applied Physics **117**, 044505 (2015).
[19] O. Olikh, Ultrasonics **56**, 545 (2015).
[20] V. N. Pavlovich, phys. stat. sol. (b) **180**, 97 (1993).
[21] F. Mirzade, J. Appl. Phys. **110**, 064906 (2011).
[22] R. Peleshchak, O. Kuzyk, and O. Dan'kiv, Ukr. J. Phys. **61**, 741 (2016).
[23] V. D. Krevchik, R. A. Muminov, and A. Y. Yafasov, phys. stat. sol. (a) **63**, K159 (1981).
[24] F. Mirzade, J. Appl. Phys. **97**, 084911 (2005).
[25] I. Ostrovskii and O. Korotchenkov, Solid State Commun. **82**, 267 (1992).
[26] O. Olikh and K. Voytenko, Ultrasonics **66**, 1 (2016).
[27] N. Guseynov, Y. Olikh, and S. Askerov, Tech. Phys. Lett. **33**, 18 (2007).
[28] P. Parchinskii, S. Vlasov, and L. Ligai, Semiconductors **40**, 808 (2006).
[29] A. Gorb, O. Korotchenkov, O. Olikh, and A. Podolian, IEEE Trans. Nucl. Sci. **57**, 1632 (2010).
[30] A. O. Podolian, A. B. Nadtochiy, and O. A. Korotchenkov, Tech. Phys. Lett. **38**, 405 (2012).
[31] Y. Olikh, M. Tymochko, and A. Dolgolenko, Tech. Phys. Lett. **32**, 586 (2006).
[32] Y. Olikh and M. Tymochko, Tech. Phys. Lett. **37**, 37 (2011).
[33] H. Jafari and S. Feghhi, Nucl. Instrum. Methods Phys. Res., Sect. A **816**, 62 (2016).
[34] Y. P. Rao, K. Praveen, Y. R. Rani, A. Tripathi, and A. G. Prakash, Nucl. Instrum. Methods Phys. Res., Sect. B **316**, 205 (2013).
[35] M. Moll, H. Feick, E. Fretwurst, G. Lindström, and C. Schütze, Nucl. Instrum. Methods Phys. Res., Sect. A **388**, 335 (1997).
[36] J. Srour, C. Marshall, and P. Marshall, IEEE Trans. Nucl. Sci. **50**, 653 (2003).
[37] I. Pintilie, G. Lindstroem, A. Junkes, and E. Fretwurst, Nucl. Instrum. Methods Phys. Res., Sect. A **611**, 52 (2009).
[38] N. Arutyunov, N. Bennett, N. Wight, R. Krause-Rehberg, V. Emtsev, N. Abrosimov, and V. Kozlovski, phys. stat. sol. (b) **253**, 2175 (2016).
[39] C. A. Londos, G. Antonaras, and A. Chroneos, J. Appl. Phys. **114**, 193513 (2013).
[40] A. Schenka and U. Krumbein, Journal of Applied Physics **78**, 3185 (1995).
[41] S. Steingrube, O. Breitenstein, K. Ramspeck, S. Glunz, A. Schenk, and P. P. Altermatt, Journal of Applied Physics **110**, 014515 (2011).
[42] V. Gopal and S. Gupta, IEEE Trans. Electron Devices **50**, 1220 (2003).
[43] V. Gopal and S. Gupta, IEEE Trans. Electron Devices **51**, 1078 (2004).
[44] A. Akkerman, J. Barak, M. Chadwick, J. Levinson, M. Murat, and Y. Lifshitz, Radiat Phys Chem **62**, 301 (2001).
[45] D. Bräunig and F. Wulf, Radiat. Phys. Chem. **43**, 105 (1994).
[46] A. B. Sproul and M. A. Green, J. Appl. Phys. **73**, 1214 (1993).
[47] D. K. Schroder, *Semiconductor Material and Device Characterization*, 3rd ed. (John Wiley & Sons, New Jersey, 2006).
[48] A. McEvoy, T. Markvart, and L. Castaner, eds., *Solar Cells. Materials, Manufacture and Operation*, 2nd ed. (Academic

Press, Oxford, 2013).
[49] K. Wang and M. Ye, Solid-State Electron. **53**, 234 (2009).
[50] D. Schroder, IEEE Trans. Electron Devices **29**, 1336 (1982).
[51] H. Aharoni, T. Ohmi, M. M. Oka, A. Nakada, and Y. Tamai, J. Appl. Phys. **81**, 1270 (1997).
[52] A. S. H. van der Heide, A. Schonecker, J. H. Bultman, and W. C. Sinke, Progress in Photovoltaics: Research and Applications **13**, 3 (2005).
[53] J. Beier and B. Voss, in *Proceedings of the 23rd IEEE Photovoltaic Specialists Conference* (1993) pp. 321–326, Louisville, KY, USA.
[54] J. M. Shah, Y.-L. Li, T. Gessmann, and E. F. Schubert, J. Appl. Phys. **94**, 2627 (2003).
[55] A. Kaminski, J. J. Marchand, H. E. Omari, A. Laugier, Q. N. Le, and D. Sarti, in *Proceedings of the 25th IEEE Photovoltaic Specialists Conference* (1996) pp. 573–576, Washington, DC, USA.
[56] W. M. Chen, B. Monemar, E. Janzén, and J. L. Lindström, Phys. Rev. Lett. **67**, 1914 (1991).
[57] A. M. Frens, M. T. Bennebroek, A. Zakrzewski, J. Schmidt, W. M. Chen, E. Janzén, J. L. Lindström, and B. Monemar, Phys. Rev. Lett. **72**, 2939 (1994).
[58] O. Breitenstein, J. Bauer, P. P. Altermatt, and K. Ramspeck, Solid State Phenomena **156–158**, 1 (2010).
[59] T. Wosinski, A. Makosa, and Z. Witczak, Semicond. Sci. Technol. **9**, 2047 (1994).
[60] L. Chen, X. Yu, P. Chen, P. Wang, X. Gu, J. Lu, and D. Yang, Sol. Energy Mater. Sol. Cells **95**, 3148 (2011).
[61] J. Schön, A. Youssef, S. Park, L. E. Mundt, T. Niewelt, S. Mack, K. Nakajima, K. Morishita, R. Murai, M. A. Jensen, T. Buonassisi, and M. C. Schubert, J. Appl. Phys. **120**, 105703 (2016).
[62] E. Gaubas, A. Uleckas, and J. Vaitkus, Nucl. Instrum. Methods Phys. Res., Sect. A **607**, 92 (2009).
[63] I. I. Kolkovskii, P. F. Lugakov, and V. V. Shusha, phys. stat. sol. (a) **83**, 299 (1984).
[64] J. D. Murphy, K. Bothe, M. Olmo, V. V. Voronkov, and R. J. Falster, J. Appl. Phys. **110**, 053713 (2011).
[65] D. G. Thomas, J. Hopfield, and W. M. Augistyniak, Phys. Rev. **140**, A202 (1965).
[66] O. Breitenstein, J. P. Rakotoniaina, M. H. Al Rifai, and M. Werner, Progress in Photovoltaics: Research and Applications **12**, 529 (2004).
[67] V. Gopal, J. Appl. Phys. **116**, 084502 (2014).
[68] I. Baker and C. Maxey, J. Electron. Mater. **30**, 682 (2001).
[69] A. Castaldini, D. Cavalcoli, A. Cavallini, and S. Pizzini, Phys. Rev. Lett. **95**, 076401 (2005).
[70] I. Isakova, A. Bondarenko, O. Vyvenko, V. Vdovin, E. Ubyivovk, and O. Kononchuk, Journal of Physics: Conference Series **281**, 012010 (2011).
[71] X. Yu, O. Vyvenko, M. Kittler, W. Seifert, T. Mtchedlidze, T. Arguirov, and M. Reiche, Semiconductors **41**, 458 (2007).
[72] V. Kveder, M. Kittler, and W. Schröter, Phys. Rev. B **63**, 115208 (2001).
[73] M. Trushin, O. Vyvenko, T. Mchedlidze, O. Kononchuk, and M. Kittler, Solid State Phenomena **156–158**, 283 (2010).
[74] J. Lindroos and H. Savin, Sol. Energy Mater. Sol. Cells **147**, 115 (2016).
[75] T. Niewelt, J. Schöon, W. Warta, S. W. Glunz, and M. C. Schubert, IEEE Journal of Photovoltaics **7**, 383 (2017).
[76] V. Vahanissi, A. Haarahiltunen, H. Talvitie, M. Yli-Koski, and H. Savin, Progress in Photovoltaics: Research and Applications **21**, 1127 (2012).
[77] J. Schmidt, Progress in Photovoltaics: Research and Applications **13**, 325 (2005).
[78] T. Mchedlidze and J. Weber, phys. stat. sol. (b) **251**, 1608 (2014).
[79] T. Mchedlidze, L. Scheffler, J. Weber, M. Herms, J. Neusel, V. Osinniy, C. Moller, and K. Lauer, J. Appl. Phys. **103**, 013901 (2013).
[80] J. Murphy, J. McGuire, K. Bothe, V. Voronkov, and R. Falster, Sol. Energy Mater. Sol. Cells **120**, 402 (2014).
[81] J. D. Murphy, K. Bothe, R. Krain, V. V. Voronkov, and R. J. Falster, J. Appl. Phys. **111**, 113709 (2012).
[82] M. Porrini and P. Tessariol, Materials Science and Engineering B **73**, 244 (2000).
[83] W. Wijaranakula, J. Etectrochem. Soc. **140**, 275 (1993).
[84] G. Lindström, M. Ahmed, S. Albergo, P. Allport, D. Anderson, L. Andricek, M. Angarano, V. Augelli, N. Bacchetta, P. Bartalini, R. Bates, U. Biggeri, G. Bilei, D. Bisello, D. Boemi, E. Borchi, T. Botila, T. Brodbeck, M. Bruzzi, T. Budzynski, P. Burger, F. Campabadal, G. Casse, E. Catacchini, A. Chilingarov, P. Ciampolini, V. Cindro, M. Costa, D. Creanza, P. Clauws, C. Da Via, G. Davies, W. De Boer, R. DellOrso, M. De Palma, B. Dezillie, V. Eremin, O. Evrard, G. Fallica, G. Fanouraki, H. Feick, E. Focardi, L. Fonseca, E. Fretwurst, J. Fuster, K. Gabathuler, M. Glaser, P. Grabiec, E. Grigorievt, G. Hall, M. Hanlond, F. Hauler, S. Heising, A. , Holmes-Siedle, R. Horisberger, G. Hughes, M. Huhtinen, I. Ilyashenko, A. Ivanov, B. Jones, L. Jungermann, A. Kaminsky, Z. Kohout, G. Kramberger, M. Kuhnke, S. Kwan, F. Lemeilleur, C. Leroy, M. Letheren, Z. Li, T. Ligonzo, V. Linhart, P. Litovchenko, D. Loukas, M. Lozano, Z. Luczynski, G. Lutz, G. MacEvoy, S. Manolopoulos, A. Markou, C. Martinez, A. Messineo, M. Mikuž, M. Moll, E. Nossarzewska, G. Ottaviani, V. Oshea, G. Parrini, D. Passeri, D. Petre, A. Pickford, I. Pintilie, L. Pintilie, S. Pospisil, R. Potenza, C. Raine, J. Rafi, P. Ratoff, H. Richter, P. Riedler, S. Roe, P. Roy, A. Ruzin, A. Ryazanov, A. Santocchia, L. Schiavulli, P. Sicho, I. Siotis, T. Sloan, W. Slysz, K. Smith, M. Solanky, B. Sopko, S. K., B. Sundby Avset, S. B., C. Tivarus, G. Tonelli, A. Tricomi, S. Tzamarias, G. Valvo, A. Vasilescu, A. Vayaki, E. Verbitskaya, P. Verdini, V. Vrba, S. Watts, E. Weber, M. Wegrzecki, I. Wegrzecka, P. Weilhammer, R. Wheadon, C. Wilburn, I. Wilhelm, R. Wunstorf, J. Wüstenfeld, J. Wyss, K. Zankel, P. Zabierowski, and D. Žontar, Nucl. Instrum. Methods Phys. Res., Sect. A **406**, 308 (2001).
[85] I. Pintilie, G. Lindstroem, A. Junkes, and E. Fretwurst, Nucl. Instrum. Methods Phys. Res., Sect. A **611**, 52 (2009).
[86] M. Moll, *Radiation damage in silicon particle detectors: Microscopic defects and macroscopic properties*, Ph.D. thesis, Universität Hamburg (1999).
[87] J. Stahl, E. Fretwurst, G. Lindström, and I. Pintilie, Nucl. Instrum. Methods Phys. Res., Sect. A **512**, 111 (2003).
[88] I. I. Kolkovskii and V. Lukyanitsa, Semiconductors **31**, 340 (1997).
[89] R. Siemieniec, W. Sudkamp, and J. Lutz, in *Proceedings of the Fourth IEEE International Caracas Conference on Devices, Circuits and Systems* (Oranjestad, Aruba, Netherlands, 2002) pp. D029–1–D029–6.
[90] S. D. Brotherton and P. Bradley, J. Appl. Phys. **53**, 5720 (1982).
[91] V. P. Markevich, A. R. Peaker, S. B. Lastovskii, L. I. Murin, J. Coutinho, V. J. B. Torres, P. R. Briddon, L. Dobaczewski, E. V. Monakhov, and B. G. Svensson, Phys. Rev. B **80**, 235207 (2009).
[92] H. Bleichner, P. Jonsson, N. Keskitalo, and E. Nordlander, J. Appl. Phys. **79**, 9142 (1996).
[93] E. Fretwurst, F. Hönniger, G. Kramberger, G. Lindström, I. Pintilie, and R. Röder, Nucl. Instrum. Methods Phys. Res., Sect. A **583**, 58 (2007).
[94] L. C. Kimerling, M. Asom, J. Benton, P. Drevinsky, and C. Caefer, Materials Science Forum **38–41**, 141 (1989).
[95] L. W. Song, X. D. Zhan, B. W. Benson, and G. D. Watkins, Phys. Rev. B **42**, 5765 (1990).
[96] J. L. Benton, S. Libertino, P. Kringhøj, D. J. Eaglesham, J. M. Poate, and S. Coffa, J. Appl. Phys. **82**, 120 (1997).
[97] S. Coffa, V. Privitera, F. Priolo, S. Libertino, and G. Mannino, J. Appl. Phys. **81**, 1639 (1997).
[98] N. Ganagona, B. Raeissi, L. Vines, E. V. Monakhov, and B. G. Svensson, phys. stat. sol. (c) **9**, 2009 (2012).

[99] L. Vines, E. V. Monakhov, A. Y. Kuznetsov, R. Kozłowski, P. Kaminski, and B. G. Svensson, Phys. Rev. B **78**, 085205 (2008).

[100] L. I. Murin, V. P. Markevich, I. F. Medvedeva, and L. Dobaczewski, Semiconductors **40**, 1282 (2006).

[101] B. N. Mukashev, K. A. Abdullin, and Y. V. Gorelkinskii, Physics–Uspekhi **43**, 139 (2000).